Production of runaway electrons and x-rays during streamer inception phase

Luis Contreras-Vidal* , Caitano L da Silva and Richard G Sonnenfeld

Department of Physics and Langmuir Lab, New Mexico Institute of Mining and Technology, Socorro, NM 87801, United States of America

E-mail: luis.contrerasvidal@student.nmt.edu

Received 25 September 2022, revised 30 November 2022 Accepted for publication 12 December 2022 Published 28 December 2022



Abstract

Streamers play a key role in the formation and propagation of lightning channels. In nature streamers rarely appear alone. Their ensemble behavior is very complex and challenging to describe. For instance, the intricate dynamics within the streamer zone of negative lightning leaders give rise to space stems, which help advance the stepped-leader. Another example is how the increasing morphological complexity of sprites can lead to higher sprite current and greater energy deposition in the mesosphere. Insights into the complex dynamics of a streamer corona can be obtained from laboratory experiments that allow us to control the conditions of streamer formation. Based on simultaneous nanosecond-temporal-resolution photography, and measurements of voltage, current, and x-ray emissions, we report the characteristics of negative laboratory streamers in 88 kPa of atmosphere. The streamers are produced at peak voltages of $62.2 \pm 3.8 \,\mathrm{kV}$ in a point-to-plane discharge gap of 6 cm. While all discharges were driven to the same peak voltage, the discharges occurred at different stages of the relatively slow voltage rise (177 ns), allowing us to study discharge properties as a function of onset voltage. The onset voltage ranged between 24 and 67 kV, but x-ray emissions were observed to only occur above 53 kV, with x-ray burst energies scaling quadratically with voltage. The average delay between the current pulse and x-ray emission was found to be 3.5 ± 0.5 ns, indicating that runaway electrons are produced during the streamer inception phase or no later than the transition stage, when the inception cloud is breaking into streamer filaments. During this short time span, runaway electrons can traverse the gap, hit the ground plate and produce bremsstrahlung x-ray photons. However, streamers themselves cannot traverse more than 3.5 mm across the gap, which supports the idea that runaway electron production is not associated to streamer connection to the ground electrode.

Keywords: streamers, x-rays, plasma, lightning, runaway electrons, high voltage discharge

(Some figures may appear in colour only in the online journal)

1. Introduction

A lightning leader propagates by creating a field enhancement at its tip, which allows the leader to penetrate regions where the background field would normally be too low for efficient ionization to occur [14, 31]. Lightning leaders create the

pathway for cloud-to-ground lightning to occur and partially discharge thunderclouds. While the measurements obtained in field experiments are undeniably authentic if one's goal is to understand natural lightning, the easy repeatability and fine-grained control of laboratory experiments can help us gain a deeper insight into the physics of lightning leaders. Though quite different in temporal and spatial scales, lightning and laboratory air-plasma discharges obey comparable fundamental physical principles [30]. Optical observations

^{*} Author to whom any correspondence should be addressed.

associated with sprite streamers and optical emissions from laboratory discharges also have many important similarities [8, 25].

A key similarity can be observed, for instance, in the x-ray emissions from lightning [10, 13, 16, 20] and laboratory discharges [12, 18, 30]. Cold runaway electron acceleration is the most plausible mechanism capable of explaining the production of x-rays during the lightning stepping process [5, 9] and in centimeter- to meter-long laboratory discharges [17, 30]. However, the details of how this mechanism takes place in the complex streamer zone of negative lightning channels is yet to be understood. This idea has been generalized with a suggestion that runaway electrons may be a universal process in all electrical discharges [30], but it remains unclear if runaway electrons are a mere consequence of high electric fields produced at the electrical discharge ionization front, or if they impact the discharge formation and propagation [24].

While the study of x-ray emission by laboratory discharges is plentiful, time-resolved observations on the precise moment of x-ray emission are scarce. Dwyer *et al* [12] showed that during simultaneous microsecond-time-resolved measurements of voltage, current, and x-rays, x-ray pulses were observed during the peak voltage and near the time when the current is at its peak, when the voltage in the gap collapses. Although this work provided evidence of x-ray emission from laboratory sparks, their experiment lacked the temporal resolution to provide the exact point in time of the x-ray production.

More recent work by Kochkin *et al* [17, 18] with a ten-nanosecond time resolution established the connection between counterpropagating negative and positive streamers as the moment of x-ray generation. Meanwhile, work by da Silva *et al* [30] supported the idea that runaway electrons and their bremsstrahlung x-rays can be produced at voltages as low as 100 kV, with no need for counterpropagating streamers.

In this manuscript, we provide additional insight into the timing of runaway electron production and x-ray emission by streamer discharges. We demonstrate that the current rise, runaway electrons, and x-rays are produced during the streamer inception or no later than when the inception cloud [3, 23] is breaking into streamer filaments. Additionally, we report on the x-ray production threshold and its energy scaling with applied voltage.

2. Methodology

2.1. Spark gap

The Langmuir Spark Lab is a laboratory research facility on the New Mexico Tech campus. It is located in Socorro, NM where air pressure and density are roughly 87% of the mean-sea-level values (88 kPa). The lab includes a $3\,\mathrm{m}\times4\,\mathrm{m}\times2.5\,\mathrm{m}$ Faraday cage to suppress electromagnetic induction (EMI) from spark phenomena. The experiment was performed in an open room (i.e. without a pressure or vacuum chamber), at standard room temperatures (293–298 K). To supply the voltage, a Northstar 85 kV solid state trigger impulse generator delivered a voltage impulse with $176.5\pm4.1\,\mathrm{ns}$ risetime. Hereafter, the nomenclature AVG \pm STD represents average

(AVG) plus or minus one standard deviation (STD). Since this is a study of negative streamers, in all cases the impulse generator is driven negative to ground so that the copper point is a cathode and the steel ground plate an anode. The impulse generator was set to a *negative* open circuit voltage of 65 kV for all the trials in this experiment, and the resulting peak voltage was measured to be 62.2 ± 3.8 kV. Absolute voltage values are reported hereafter for simplicity.

The spark gap consists of a point-to-plane configuration. The point was machined from an 11 mm diameter copper rod that is tapered in a cone shape over its lower 25 mm. On the bottom of this cone a roughly 0.5 mm radius of curvature tip was created. A very sharp tip was explicitly avoided to improve the repeatability of our experiments, since a sharp tip deteriorates after heavy use. Detents and a set screw allow for easy adjustment of the gap in increments of 5 mm for gap lengths of 0 to 100 mm. The gap size used in these experiments was 60 mm, as shown in figure 1.

2.2. Sensors

Four sensors were connected for every experimental run.

- Voltage 1: A Northstar 2000:1 high-voltage probe (PVM-100) with a 100 kV dynamic range and a 3 ns rise time measured the voltage across the gap.
- Voltage 2: A Magnelab current-transformer with a 200 Amp dynamic range and a 48 Hz to 100 MHz flat bandpass (CT-D0.5-B) measured current into the bottom electrode. It was intentionally placed near ground to prevent arcing to the sensor.
- Voltage 3: To image the discharges, a 4Picos ICCD camera was placed inside the Faraday cage at a distance of 38 cm from the gap perpendicular to the streamer-developing axes. The Stanford Computer Optics 4Picos camera takes a single picture of the discharge, but it can control when the shutter opens and closes with subnanosecond precision. A 50 mm focal length lens was used, resulting in a field of view that covered the full gap, including both electrodes. The camera parameters and optical system remained the same during the experiment, with exception of the exposure time which varied between 10 ns and 400 ns.
- Voltage 4: A LaBr₃:Ce scintillation detector manufactured by Saint-Gobain was mounted inside the Faraday cage to detect the x-ray emissions. The scintillator has a fast primary rise/decay time of 16/54 ns. Three standard radioactive sources (Ba-133, Cd-10, Co-57) were selected to calibrate and test the linear response of the LaBr₃:Ce detector [35]. All sources were placed at 10 cm from the detector.

2.3. Data acquisition

A four-channel LeCroy HDO6014a oscilloscope with a sampling rate of 10 GHz was used to simultaneously record the voltage, current, and x-ray signals. The trigger output of

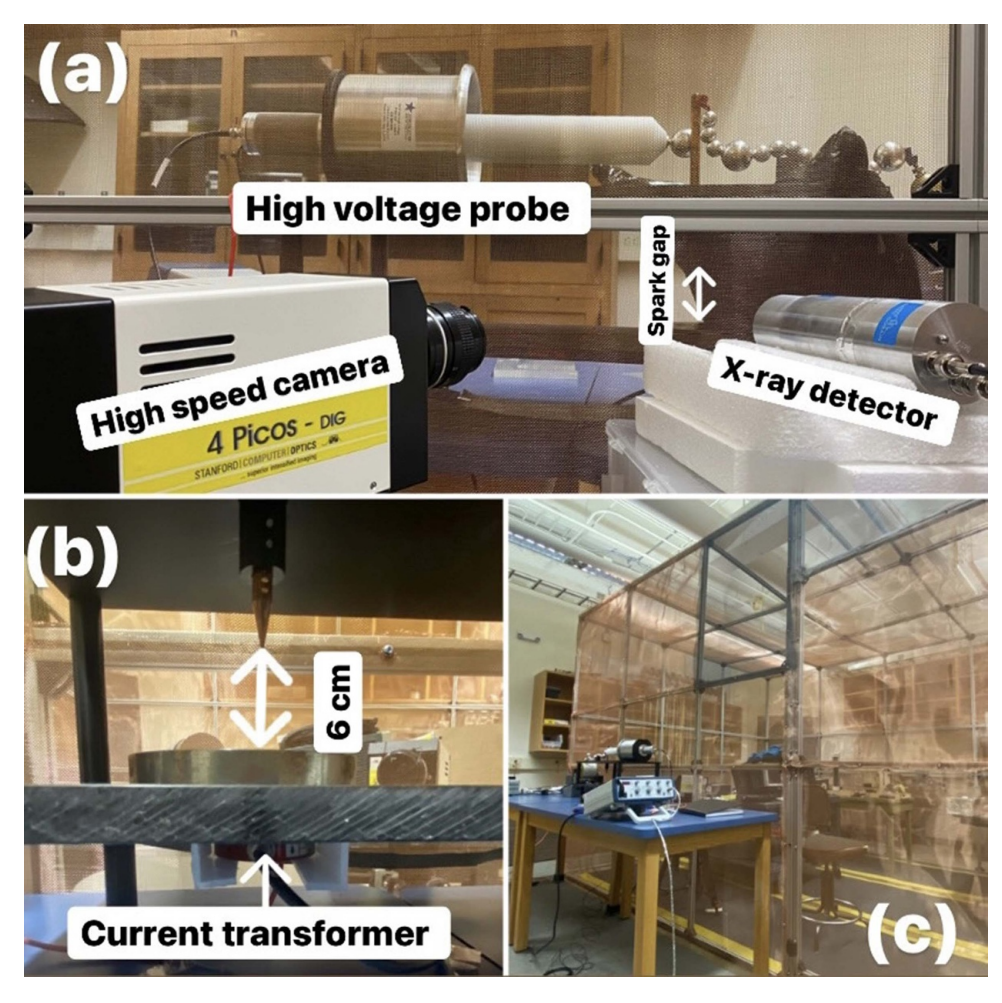


Figure 1. Experimental setup used includes: 6 cm point-to-plane discharge gap, $\pm 85 \, \text{kV}$ impulse generator, high-voltage probe, intensified fast camera, LaBr x-ray (scintillation) detector (a); and current transformer (b). The camera, x-ray detector, and data acquisition systems were enclosed inside a Faraday cage (c).

this oscilloscope was also used to trigger the camera. The voltage signal was used to coordinate all of the other measurements. The oscilloscope typically recorded a 100 ns pretrigger and a 600 ns post-trigger (see figure 4). The voltage at which the trigger level was set was varied to advance or retard the camera shutter relative to the other measurements. In this way, we were able to 'walk' the imaging window across the entire streamer process. The oscilloscope, x-ray detector, and the camera were enclosed in the Faraday cage, while the spark gap, impulse generator, voltage, and current probes were outside of the cage.

2.4. X-ray calibration

Figure 2(a) shows a sample x-ray energy spectrum collected for a Ba-133 gamma in an 8 min interval. In this example, the voltage at which the 30.85 and 81 keV energy peaks of the Ba-113 source happen are clearly distinguishable. For the three sources used (Ba-133, Cd-10, Co-57), the relation between the oscilloscope voltage and the x-ray energy is linear across

the range of interest, as shown in figure 2(b). Using additional sources, such as Na-22 and Co-60 (not shown), we have also verified that the detector has linear response all the way to the MeV energy range. The precise centroid of the line emission was obtained by fitting a Gaussian curve to the recorded spectrum, as exemplified in figure 2(a).

In order to ensure that the x-rays measured from the laboratory discharges are indeed true x-rays and not electromagnetic noise induced in the measurement system, data collection was performed with a control detector. The control, or 'dummy', detector was also manufactured by Saint-Gobain, with the only difference being that it does not contain the LaBr₃:Ce scintillating crystal. A total of 50 discharges were recorded with the control detector, without any evidence of electromagnetic noise manifesting itself in any way that could be confused with an x-ray detection. The noise root mean square (RMS) level in the dummy detector was 5 mV, which according to figure 2, amounts to an energy level of 2 keV, which is substantially lower than the typical energies measured here, of the order of hundreds of keV.

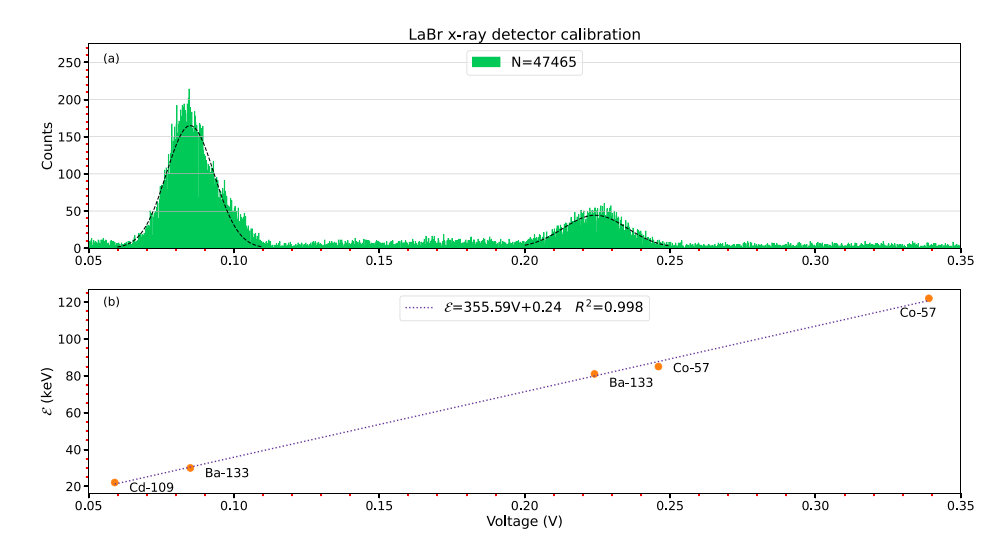


Figure 2. (a) Ba-133 spectrum from over 45 000 x-ray photons recorded in 8 min with a bin resolution of 0.19 mV. Gaussian functions (black dashed lines) were fitted to find the corresponding voltage for tabulated energy peaks. (b) The process is repeated for three standard radioactive sources (Ba-133, Cd-10, Co-57) and the LaBr detector calibration was obtained. The detector response is linear in the energy range of interest.

2.5. Timing corrections and uncertainty

In order to draw useful conclusions about nanosecondscale processes, all systematic time offsets must be properly accounted for. The timing correction implemented for each of the instruments is listed in table 1. The reference $t_0 = 0$ time was set as the onset of the voltage pulse, since the high-voltage probe cable length (ℓ_V) is the longest of all the instrument cables. Therefore, the signals on the current transformer cable (ℓ_I) and the LaBr detector cable (ℓ_{γ}) are expected to arrive earlier than expected and need to be shifted forward in time (yielding a positive offset in table 1). The cable delays and signal propagation speeds were measured using pulse reflection. Because not all cables used the same dielectrics, the values obtained ranged from 65% to 75% of the speed of light in a vacuum. Other positive corrections listed in table 1 account for the delay to trigger the camera (internal and external) and the electron transit time in the Hamamatsu R6231 photomultiplier tube (PMT) attached to the x-ray detector. The small negative corrections listed in the table account for the time of flight of photons from source to detector.

While the gap voltage was used to trigger the oscilloscope, the more scientifically interesting edge in the experiments was the current onset. The lower panels of figure 3 show that all current waveforms began with a very sharp rising edge (or falling drop, actually, since they are negative) and it is useful to define the moment when that drop begins as the current onset. To determine the onset time precisely, we employed a zero-intercept technique. First a line was fit to the 10%–90% 'rise' time of the leading edge. Second, we define the current onset time as the instant when the linear trend intercepts the zero level of the signal. This technique is more tolerant of measurement noise than a simple threshold or zero-crossing algorithm. The 'current onset time' will be important in the discussion which follows.

Table 1. Timing corrections for all the instruments used. Corrections marked with an "*" were given by the manufacturer through personal correspondence. The symbols ℓ , d, v, and c, indicate cable length, detector distance, speed of signal in the cable, and speed of light in a vacuum, respectively.

Instrument	Description	Value
4Picos high-speed camera	Time of flight of photons	$d_{4\text{Picos}}/c = -1.26\text{ns}$
	*Shutter opening delay	65 ns
	Trigger delay due to cable length	5.5 ns
Saint-Gobain LaBr x-ray detector	Delay due to cable length difference	$\frac{\ell_V}{v_V} - \frac{\ell_\gamma}{v_\gamma} = 14.7 \text{ns}$
	Time of flight of x-ray photons	$d_{\rm LaBr}/c = -0.86\rm ns$
Hamamatsu PMT	*Transit time	48 ns
Magnelab current transformer	Delay due to cable length difference	$\frac{\ell_V}{\nu_V} - \frac{\ell_I}{\nu_I} = 4.6 \text{ns}$

After discussing corrections, it is reasonable to discuss uncertainty. Given the high quality oscilloscope and pulse generators used in the cable delay measurements, the cable length uncertainty is sub-nanosecond. We did not experimentally verify the manufacturer's published 48 ns correction for the Hamamatsu PMT. However the 0.5 ns scatter in measured x-ray delays suggests that whatever the delay is it is extremely reproducible. Likewise, we did not verify the manufacturers trigger delay of 65 ns for the camera. The 5 ns uncertainty in that specification (60–65 ns) may well dominate our timing errors. With regard to x-ray measurements, the x-ray, current, and voltage signals were all simultaneously digitized. Thus, to the extent that the 48 ns figure can be believed, our conclusions about x-ray delays are nanosecond accurate.

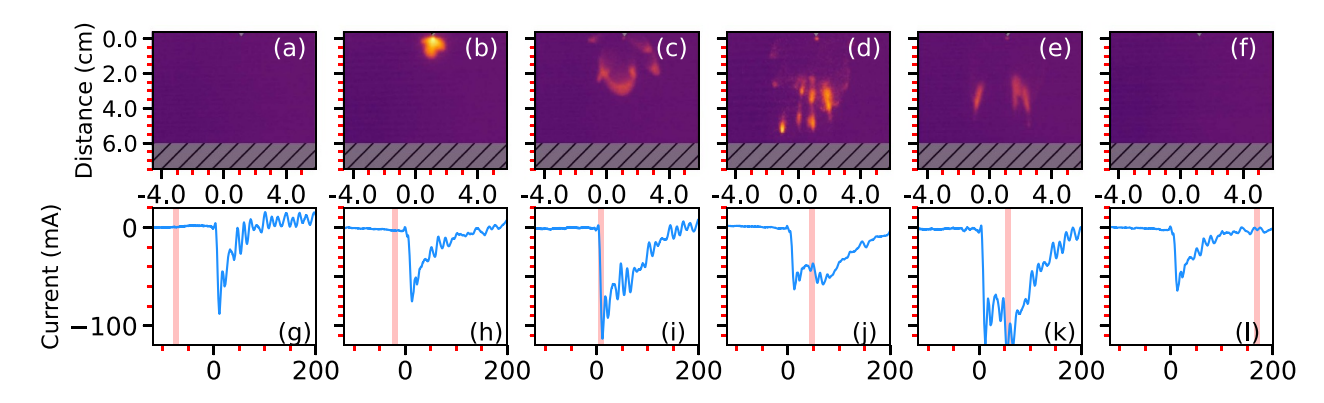


Figure 3. Time lapse of the discharge dynamics using 10 ns exposure photographs from different discharges. Panels (a)–(f) show the development of the discharge, while panels (g)–(l) show in which stage of the corresponding current pulse the photograph takes place.

2.6. Signal processing of the current waveform

The measured current waveforms of the streamers had two confounding signals which were removed for clearer analysis. The first was an effect of displacement current. Even in a vacuum, with no plasma activity, a sharply rising voltage applied to the pointed cathode would result in a displacement current at the counter electrode. Fortunately, it is rather easy to subtract this effect off. We first calculated the capacitance of our system in the absence of plasma by approximating it as a conducting rod with a hemispherical end, perpendicular and separated from a conducting plane, per the formula of Longcope [19]:

$$C = \frac{4\pi\epsilon_o a^2/h}{\sqrt{[1 - (a/h)^2] - (1 - a/h)}},$$
 (1)

where a is the diameter of the conductor, h is the gap length, and ε_o is the permeability of free space. The capacitance was calculated to be C=0.58 pF. The capacitance information can be used for subtraction of displacement current effects, where the displacement current is given as $I_d = C \frac{\mathrm{d}V}{\mathrm{d}t}$ and to calculate the electrostatic energy available before the discharge begins $(U=\frac{1}{3}CV^2)$.

In fact, when the apparatus was arranged to suppress a streamer discharge and measured data was used for I_d and $\frac{\mathrm{d}V}{\mathrm{d}t}$, the value $C_{\mathrm{fit}}=0.60\,\mathrm{pf}$ was calculated; in good agreement with equation (1). This value was then used to subtract the displacement term from all waveforms. Furthermore, although the capacitance varies during the discharge, this dynamic capacitance is already built into our current signal. We considered it appropriate to subtract the displacement current based on the static capacitance and leave the dynamic capacitance effects in the presented data.

Also, the current measurements displayed a noticeable 72 MHz component, indicative of resonance in an *RLC* circuit. We believe this resonance is an artifact of the step-response of the current sensor. Regardless of its origin, the current signals were processed with a digital low-pass filter to remove this resonance. Figure 4(b) shows in blue a typical raw current waveform and in red the processed waveform with the displacement current and the 72 MHz resonance suppressed.

3. Results and discussion

3.1. Typical discharge dynamics

A total of 148 negative discharges with peak applied voltages of $62.8\pm3.3\,\mathrm{kV}$ were produced. Figure 3 shows a composite time-lapse of the discharge dynamics using imagery from different discharges. The top panels correspond to the 4Picos imagery and the bottom panel corresponds to the measured current for each discharge. The false colors in the images indicate the light intensity. A consistent color scale is used for all the images presented herein. All frames in figure 3 were taken with a 10 ns exposure, indicated as a light-pink rectangle overlaying the current measurements shown in the bottom row of the figure ¹.

Figures 3(g)-(1) display the discharge current, which has been corrected for displacement current, as discussed in the signal processing section above. The 72 MHz component, which is particularly visible in panels (g), (i), and (k), has not yet been removed from this data. Although each panel differs in detail, they have the following characteristics in common. They begin with a sharp drop (or in absolute value terms, a sharp rise). The mean risetime of this drop was found to be $t_{\rm rc} = 4.12 \pm 0.4$ ns. We will refer to the four nanosecond period of this current rise as the 'current surge'. The very beginning of this rise (t = 0 in figure 3), will be referred to as the 'current onset'. The precise time of current onset via the zero-intercept method discussed previously. The current surge is followed by a decay with a duration of roughly 150 ns. The waveforms of figure 3 generally show a monotonic decay, but two of them, panels (j) and (k), show a 'knee' feature in the first 80 ns which will be discussed further later. In further discussion, the entire current waveform between zero crossings will be referred to as the 'current pulse'.

Referring now to the images in figures 3(a)–(f), we note that (a) shows no evidence of a discharge and the camera shutter is opened well before the current onset. In (b), we note that

¹ Data collected for all the 148 discharges and the control discharges with photographs with exposures ranging between 10 ns to 400 ns has been made available online [7].

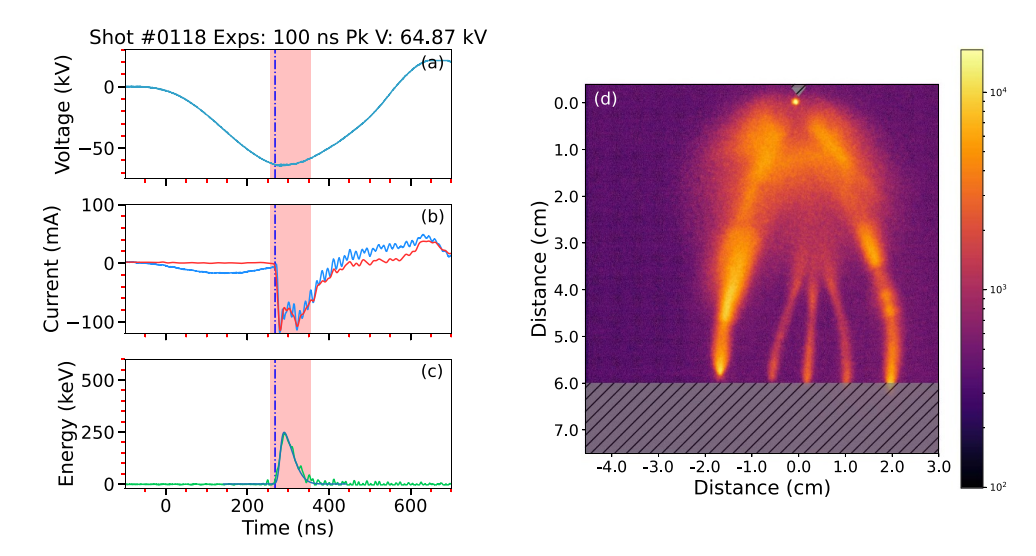


Figure 4. Streamers with x-ray emission. (a) Applied voltage. (b) Filtered discharge current (red curve) and measured current (blue). The vertical blue dot-dashed line corresponds to the current onset. (c) Detected x-ray pulse and its fit in blue. (d) 100 nanosecond exposure photo of the electrical discharge. A similar figure produced for each one of the 148 discharges recorded can be found in the data repository [7].

there is an 'inception cloud' [3, 22], which appears about 15 ns before the current onset and surge. One might expect that there should be no cloud without a corresponding current, but we have explicitly not adjusted the timing of our data to fulfill this expectation. The times presented are our best estimates of the correct times for all sensors per the timing analysis presented above. As discussed above we do not believe that the synchronization error between current and image exceeds 5 ns, but we have not completely ruled out a larger error. In (c), there is clearly a filamentary streamer, and it corresponds well with the current surge. In (d) and (e), the current persists and the streamer fronts have advanced further across the gap. In panel (f), the current is clearly zero and the streamer discharges has ceased emitting visible light.

Accounting for all possible sources of temporal uncertainty, we conclude that the current surge after t = 0 marks either the discharge inception (panel (a)) or the transition from a relatively uniform inception cloud into a filamentary streamer corona [23] (panel (b)). Some uncertainty is expected since the inception stage lasts tens of nanoseconds [22]. When current peaks the streamers have not traveled more than halfway across the gap (figures 3(c) and (i)), and thus the current surge is not related to the connection to the ground electrode. The current pulse width is indicative of the propagation time of streamers across the gap, and the current collapses shortly after that. The brief rise time of the current surge indicates that it is not related to streamer connection. If the surge were caused by streamer connection to the ground (anode) electrode, the streamer would need to have unrealistically high speeds in order to traverse the gap in 4 ns.

In figure 3 we have provided a quick glance to the discharge dynamics. In the next sections we will go into a more detailed description of these discharges. In particular, we show that although all discharges were driven by the impulse generator set to the same voltage, the discharges occurred at different

stages of the rising voltage pulse. This spread of the discharge onset voltage (the voltage at the instant of current onset) leads to four different categories of streamers: streamer with and without x-ray emissions, and streamer that connect or do not connect to the ground electrode. These four different categories can be distinguished by two independent discharge thresholds: a threshold for x-ray production, and a *lower* threshold for connection to ground.

3.2. Timing and context of x-ray emissions

3.2.1. Streamers with x-ray emission. In this particular experimental setup, x-ray emissions are detected in streamer discharges for which current onset occurred at voltages greater than $V_{\gamma} = 53.3$ kV. Figure 4 shows an example of a discharge with x-ray emission photographed with a 100 ns exposure. As in figure 3, the exposure time is shown as a light-pink rectangle overlaying the time series plots. Figure 4(a) presents the driving voltage V. Figure 4(b) shows the raw measured current (blue curve) and the processed discharge current (red). As discussed, both the displacement current and a 72 MHz oscillation have been processed out of the raw data. Processing the current waveform helped us obtain a more precise measurement of the entire current pulse's full-width at halfmaximum (FWHM). The vertical dotted-dashed line in panels (a)–(c) indicates the precise time of current onset, as defined above.

Figure 4(c) shows the detected x-ray burst. On average, the x-ray bursts were detected at $t_{\gamma} = 3.53 \pm 0.51$ ns after the current onset. The registered pulse (green curve) is superposed by the detector's single-photon, double-exponential function response (blue curve). In this particular case the x-ray burst energy is 250 keV, a value which far exceeds the energy a single electron could gain from the available potential difference (65 kV). This must be a result of photon pile-up,

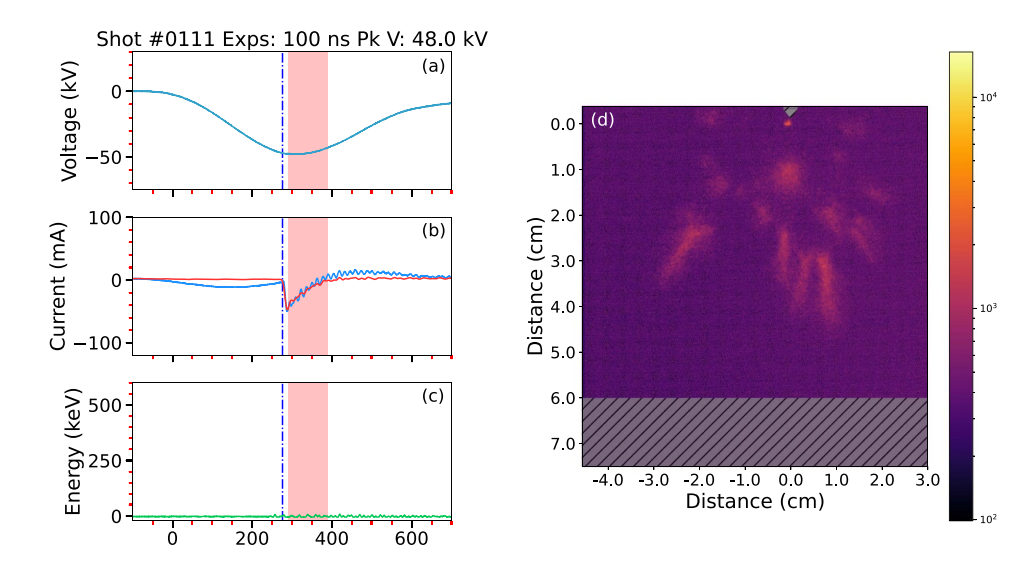


Figure 5. Streamers without x-ray emission. (a) Voltage. (b) Current. (c) No evidence of x-ray detection. (d) Photograph (100 ns exposure). The figure has the same layout as in figure 4.

i.e. several photons are produced and arrive simultaneously at the detector [24, 30]. In order for the resulting energy pulse to resemble that of a single photon, the transit time spread as photons travel from source to detector must be a small fraction of the 16 ns decay time of the crystal. Figure 4(d) shows a 100 ns exposure photograph in which the streamers manage to connect to the ground electrode. However, in no cases do these streamer connections result in a spark. We know there is no spark both because of naked eye observations, long-exposure DSLR photography, and because the voltage waveform shown in panel (a) does not differ from the open circuit voltage. Also, current and voltage data was acquired for longer records of the current, beyond the 1 μ s time scale, which should be in principle sufficient to promote streamer-to-spark transition if one were present [29, 31].²

3.2.2. Streamers without x-ray emission. In contrast, and to further the argument we will make about the source of x-rays, we show data without x-ray emissions. The threshold for x-ray emissions was found to be $V_{\gamma} > = 53.3\,\mathrm{kV}$. Figure 5 shows an example of a streamer launched at 48 kV and an exposure time of 100 ns. The figure has the same format as figure 4. The only difference between figures 4 and 5 is the initiation voltage.

3.2.3. Timing of runaway electron production. Because bremsstrahlung radiation due to runaway electrons impacting the ground electrode is known to be the key process responsible for the production of laboratory x-rays on short air gaps [24, 30], we present an analysis of the transit times of runaway electrons to determine the precise moment of runaway electron

production and whether they are the likely agent for the x-ray observations we have made.

For energies above $\sim 100\,\mathrm{eV}$ in atmospheric pressure air, the cross section for electron scattering with the ambient gas decreases with increasing electron kinetic energy, this can lead to the production of so-called 'runaway' electrons [15]. For runaway electrons, the electric field supplies more energy than is lost to collisions [15, 21]. In the energy range between $300\,\mathrm{eV}$ and $300\,\mathrm{keV}$, the runaway electron threshold energy (in eV) can be approximated by equation (2) [24]:

$$K_{\rm th} = 8.4 \times 10^5 \cdot E^{-1.4} \tag{2}$$

where E is the applied electric field in kV cm⁻¹. In our experiment, x-ray emission is associated with voltages at current onset $V_{\gamma} \ge 53.3 \,\mathrm{kV}$ (which corresponds to an average electric field of $\bar{E} = 9 \,\mathrm{kV} \,\mathrm{cm}^{-1}$). Using $\bar{E} = 9 \,\mathrm{kV} \,\mathrm{cm}^{-1}$ in equation (2) as a lower bound, one calculates the lower bound runaway electron threshold energy $K_{\mathrm{th}} = 39 \,\mathrm{keV}$. This is a rough estimate, since the electric field used is an average across the gap, and not the precise electric field at the location of runaway electron acceleration. Nevertheless, runaway electrons must be upper bounded by the breakdown voltage ($E_k = 25 \,\mathrm{kV} \,\mathrm{cm}^{-1}$ with corresponding $K_{\mathrm{th}} = 9.3 \,\mathrm{keV}$). Fields higher than $25 \,\mathrm{kV} \,\mathrm{cm}^{-1}$ should not exist for long, as they will generate prolific ionization leading to field collapse [11].

At these range of energies Bremsstrahlung x-rays are only produced when energetic electrons hit the ground electrode, as verified by Monte Carlo simulations [24]. Using this range of K_{th} 's we can estimate the distance traveled across the gap (d_s) by the discharge at the moment of runaway electron production by the formula:

$$d_s = v_s(t_\gamma - t_{\rm re}), \tag{3}$$

where $v_s \simeq 10^6 \,\mathrm{m \ s^{-1}}$ is the typical streamer velocity for a $-60 \,\mathrm{kV}$ discharge [2], $t_\gamma = 3.48 \pm 0.51 \,\mathrm{ns}$ is the average

² Our apparatus is eminently capable of producing sparks, but we selected the particular gap and voltage for this study precisely because they rarely produced sparks. Figure 8 in the appendix is included to demonstrate the different behavior of the apparatus when a spark rather than a streamer is produced.

measured delay between current onset and x-ray detection, $t_{\rm re} = \frac{h-d_s}{v_{\rm re}}$ is the transit time of runaway electrons across the gap, h is the gap length, $0.7\,{\rm m\,s^{-1}} \leqslant v_{\rm re} = \sqrt{\frac{2K_{\rm th}}{m_e}} \leqslant 1.2\times 10^8\,{\rm m\,s^{-1}}$ is the range of runaway electrons' velocities without relativistic correction, and m_e is the electron mass.

Using $9.3 \, \text{keV} \le K_{\text{th}} \le 39 \, \text{keV}$, the transit time of runaway electrons can be bounded as $0.5 \, \text{ns} = \frac{h}{v_{\text{max}}} < t_{\text{re}} < \frac{h}{v_{\text{min}}} = 0.8 \, \text{ns}$, placing d_s between 2.2 and 3.5 mm.

Thus, we can confirm that runaway electrons are produced very early on, during the streamer inception stage [33, 34]. If we interpret our results as indicating that the current pulse surge corresponds to the discharge inception at the high-voltage electrode (let us call this the *lower bound* estimate), runaway electrons are produced within the inception cloud. This finding suggests that filamentary streamer channels may not be necessary for the production of runaway electrons [1, 22, 27, 28]. Additionally, contrary to previous observations [1, 22, 27, 28, 33, 34], neither low pressures, fast voltage rise times, nor pulsed discharges were necessary to achieve the type of discharges that produce runaway electrons.

The lower bound estimate (paragraph above) places the runaway electron production within the inception cloud. Alternatively, an upper bound estimate would be the interpretation that the current surge appears when the inception cloud breaks into filamentary streamers, and thus runaway electron emission would happen no later than at this time. In any case, this is well before streamers bridge the gap. That time scale can be roughly estimated as $h/v_s \simeq 60$ ns. As reported in the next section, the inferred threshold for streamer connection to the ground electrode is $V_{\rm cn} \simeq 45$ kV, which is lower than V_{γ} . Therefore, all x-ray discharges that meet the threshold to emit x-rays also meet the threshold for connection and go on to bridge the gap. Thus, to reiterate the conclusion, in our measurements, the detected x-rays are not a consequence of bremsstrahlung radiation from streamer heads directly impinging on the ground electrode. They are produced by runaway electrons produced early on during streamer inception, and that traverse the gap to collide with the ground plate.

3.3. Statistical properties, thresholds, and trends

Four different parameters and their dependence on the discharge voltage are shown in figure 6. Once again the discharge voltage is defined as the voltage at the instant of current onset. The figure shows the peak current (a), current pulse FWHM (b), x-ray energy (c), and the ratio between total x-ray energy emitted and electrical energy available in the gap. The data points use different symbols to distinguish streamers that connected or did not connect to ground, as verified by inspection of the 4Picos imagery. In some cases, connecting streamers display a 'knee' signature in the current pulse. The knee is a secondary peak which appears at 26 MHz in a Fourier decomposition of the current data. An example of the knee signature appears in figure 4(b). In figures 6, green circles represent connecting streamers ('C-streamers'), blue triangles represent connecting streamers that have the current knee signature, and

orange stars represent streamers that did not connect to the grounded electrode.

Figure 6(a) shows a weakly quadratic relation between peak current and voltage. Figure 6(b) shows that the scatter in FWHM can be used as a proxy for determining whether or not streamers bridge the gap. For non-connecting streamers, the mean FWHM is given by $FWHM_{avg} = 69.3 \pm 4.8 \text{ ns.}$ For voltages lower than 45 kV, the coefficient of variation (= STD/AVG) is 7%, while for higher voltages it is 47%. An increased spread in FWHM happens when streamers start to connect to the ground electrode and the width is affected by how much charge the streamers transfer to the ground. We can see in figure 6(b) that the largest FWHM values are a consequence of the knee signature, which may be indicative of additional charge transfer. The threshold for streamer connection $V_{\rm cn} = 45 \,\mathrm{kV}$ is defined using combined information of the imagery and of figure 6(b). According to figure 6(b), only <7% of the cases do not show a clear connection above $V_{\rm cn}$. Note that the measured value for FWHM_{avg} roughly agrees with our estimate of the streamer transit time across the gap, $h/v_s = 60 \,\mathrm{ns}$.

Figure 6(c) shows that the threshold for x-ray production is 53.3 kV, which can be determined precisely by fitting the energy versus voltage trend with a quadratic function. The quadratic trend arises because available electrical energy in the gap increases quadratically with voltage, $U = \frac{1}{2}CV^2$. In figure 6(d) we attempt to allow for this trend, by plotting the ratio between the total x-ray energy emitted to the electrical energy available in the gap (U) given as:

$$R = \Omega \frac{\varepsilon}{U},\tag{4}$$

where ε is the detected x-ray energy, and Ω is a solid-angle correction factor. This correction factor is given by

$$\Omega = \frac{4\pi d_{\text{LaBr}}^2}{A_{\text{LaBr}}} = 419, \tag{5}$$

where $A_{\rm LaBr}$ is the LaBr detector collection area and $d_{\rm LaBr}$ is its distance to the spark gap. The quantity $1/\Omega$ is the fraction of the total solid angle (4π) encompassed by the detector. Thus, $\Omega\varepsilon$ is the total x-ray energy emitted by the streamer discharge, assuming that the source is isotropic. As shown in figure 6(d), the emitted x-ray energy amounts to a fraction of 1×10^{-8} to 4×10^{-8} of the electrical energy available in the gap. Please note that the energy fraction does not increase with voltage as rapidly as the x-ray energy itself. The main message of figure 6(d) is that a streamer gap is not an efficient x-ray generator, nor is a thunderstorm!

Figure 6 emphasizes an important result: x-ray emission and streamer connection to the ground are *not* causally related. It is a coincidence that all discharges that emit x-rays also end up bridging the gap. This happens because the threshold for connection is lower than the threshold for x-ray emission in this particular setup. Another piece of evidence is that streamers with and without the current knee signature, which signifies a good connection to ground, appear uniformly distributed across voltages and x-ray energies in figure 6(d). Kochkin *et al* [17] concluded that, in meter-scale discharges, x-rays are

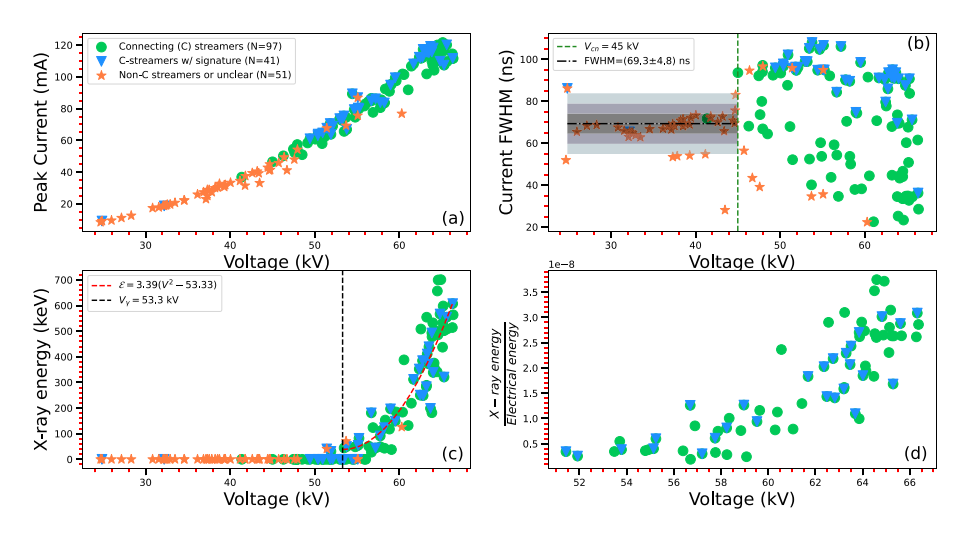


Figure 6. Dependence of key parameters on the voltage at the discharge onset. (a) Peak current. (b) Current FWHM. The threshold for streamer connection ($V_{\rm cn}=45\,{\rm kV}$) is shown as a green dashed vertical line. The gray-shaded rectangles illustrate the coefficient of variation, with each color shade being one standard deviation. (c) Detected x-ray burs energy. The threshold for x-ray production ($V_{\gamma}=53.3\,{\rm kV}$) is shown as vertical black dashed line. V_{γ} was obtained from the quadratic fit to the measurements (red dashed curve). (d) The ratio between x-ray energy and electrical energy available in the gap. Note that the energy fraction does not increase with voltage as abruptly as the x-ray energy itself.

produced when streamers attach to the ground electrode. In that setup, the attachment process involves counterpropagating streamers. We speculate that Kochkin *et al*'s conclusion may be misguided if $V_{\rm cn} < V_{\gamma}$ for their setup as well. The question of runaway electron production context can only be fully addressed by precise timing of the x-ray emissions, as has been attempted in this investigation.

Figure 7 shows histograms with the distribution of some important parameters measured: voltage at discharge onset (a), x-ray burst energy (b), current to x-ray delay (c), and current risetime (d). The figure discriminates between detections with and without x-rays. Using standard terminology in the literature [24, 30], one could state that the x-ray detection efficiency is 53%, i.e. 70 of the 148 discharges produced xrays. It is expected that not 100% of the cases should produce detectable x-rays since the probability of x-ray detection follows a Poisson distribution [4, 24]. In simpler terms, it is possible that all emitted photons manage to avoid reaching the detector in selected triggers. However, a detailed inspection of figures 6(c) and 7(a) indicates that the low detection frequency is an artifact arising from the spread in discharge voltage (between 24 and 67 kV) among all detections. Only discharges with $V > V_{\gamma}$ are expected to produce rays, and thus, for voltages greater than 53.3 kV, the actual detection frequency is 89% (68 out of 76). Pantuso et al [24] first suggested that the spread in voltage may affect the measurements, making it difficult to probe the energy distribution of runaway electrons at the source. We speculate that all previous measurements that lacked the temporal resolution to determine the voltage at the instant of runaway electron production suffer from the same problem. It is important to determine the detection frequency accurately, because it can help determine the Poisson distribution of photons arriving at the detector, and thus, help alleviate photon pile-up issues [24]. The spectrum shown in figure 7(b) is heavily influenced by photon pile up. Detected x-ray energies varied between 27 to 700 keV, with a median value of $\tilde{\varepsilon}=302$ keV. We note that the median x-ray burst energy (300 keV) exceeds the available potential energy (65 kV) by a factor of $r=\frac{300}{65}=4.6$ consistent with the interpretation of photon pile up. X-ray energies that exceed the available potential energy have been reported before. More specifically, Dwyer *et al* [12] observed x-ray energies of a 'few' MeV for 1 MV discharges (r=3–5), meanwhile Rahman *et al* [26] reported energies of 'tens' of MeV for 1 MV discharges (r>10).

Figure 7(c) shows that, despite all potential sources of temporal uncertainty, the delay between current onset and x-ray detection can be measured with a small standard deviation of 0.5 ns. This value is quite small, of the order of the runaway electron travel time across the gap. The 3.5 ns delay between current and x-ray emission indicates that runaway electrons are produced very early on during streamer inception. During this brief time interval, negative streamers cannot travel more than 3.5 mm. As discussed in the timing corrections section, the primary source of uncertainty for the delays reported in figure 7(c) is the 48 ns PMT transit time of the Saint-Gobain x-ray detector. The results shown in figure 7(c) demonstrate that the uncertainty in this quantity must be small, under 1 ns. Figure 7(d) shows that the risetime of the discharges is also quite reproducible. There is no significant difference between the two distributions for a streamer with and without x-ray emissions other than the fact that the latter case seems to have a longer tail beyond 5 ns. Additionally, there is no clear distinction in risetimes for the three categories displayed in figure 6, further emphasizing that the current rise has nothing to do with ground connection. A clear understanding of what particular process creates the current risetime depends on accurate relative timing between the camera and current sensors. In this

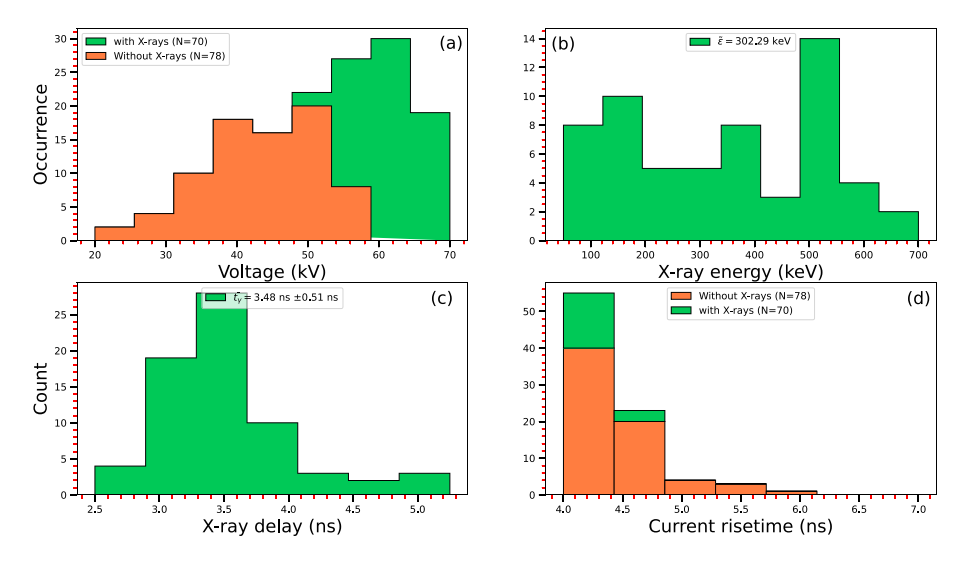


Figure 7. Histograms of important discharge parameters. (a) Voltage. (b) Ray burst energy. (c) X-ray delay after current onset. (d) Current 10%–90% risetime. In panel (a), streamers with and without x-ray emissions were triggered at median voltages of 63 and 44 kV, respectively.

case, confidence in our conclusions is limited by the uncertainty in the 65 ns internal trigger delay time of the 4Picos camera. This uncertainty should not be higher than several nanoseconds. In this brief time interval, the streamer cannot travel more than 1 cm across the gap. Therefore, we reiterate our main conclusion that the current pulse happens at streamer inception or as the inception cloud destabilizes into filaments (at the latest), and that runaway electrons are emitted immediately (~ 3 ns) after.

4. Summary and conclusions

In this experiment, the voltage impulse generator was set to 65 kV, but due to the stochasticity of the electrical breakdown process, discharges started at several different instants during the relatively slow rise of the voltage pulse, and thus, took place at different *onset* voltages. What may be seen as experimental jitter turned out to be an opportunity to study streamer properties as a function of discharge voltage.

Since streamer connections began around 45 kV, while x-ray emissions did not begin until 53 kV, which suggests that a streamer connection is not a sufficient cause for x-ray emissions. A stronger and more interesting result arises from our timing measurements. Because x-ray emissions occurred within nanoseconds of current onset, while streamer connections occurred between tens to one hundred nanoseconds later, the x-rays could not have been caused by the streamer connection to the ground electrode.

If streamer connections do not cause the x-rays, what does? Our measurements with nanosecond temporal resolution reveal that runaway electron production and x-ray emission happen early on during streamer inception. More specifically, we have bounded the moment of runaway electron emission to take place between streamer inception and the instant when the inception cloud breaks into filamentary streamers. Then runaway electrons traverse the gap in roughly 0.5 ns, collide

with the ground electrode, and produce Bremsstrahlung x-ray photons.

The threshold for streamer connection can be derived solely from looking at electrical measurements. We can easily see that for voltages larger than 45 kV, the current pulses become less reproducible, yielding a larger spread in the pulse width.

For voltages above 53.3 kV, x-ray burst energy scales quadratically with the gap voltage. It remains to be seen if this scaling law extends all the way to the megavolt potentials available in lightning [5].

Because negative streamers propagate in the direction of electron drift, while positives do not, negative and positive streamers behave in completely different ways during their deceleration and stopping process [32]. Hence, future work must include switching the polarity of the impulse generator to compare the discharge dynamics between positive and negative streamers. This future work could include obtaining 0.5 ns to 1 ns exposure imagery of the discharges to study the collapse of the inception cloud into filamentary streamers.

Data availability statement

The data that support the findings of this study are openly available at the following URL/DOI: https://figshare.com/articles/figure/Production_of_runaway_electrons_and_x-rays_during_streamer_inception_phase/20523924.

Acknowledgments

This research has been primarily supported by NSF Grant AGS-1917069 to New Mexico Tech. The Spark Lab was largely built via DURIP Grant FA9550-19-1-009 from the Air Force Office of Scientific Research. We thank Paul Clem of Sandia National Laboratories for being supportive of the DURIP proposal submission and, in general, of this research project.

Appendix. Supplementary figure

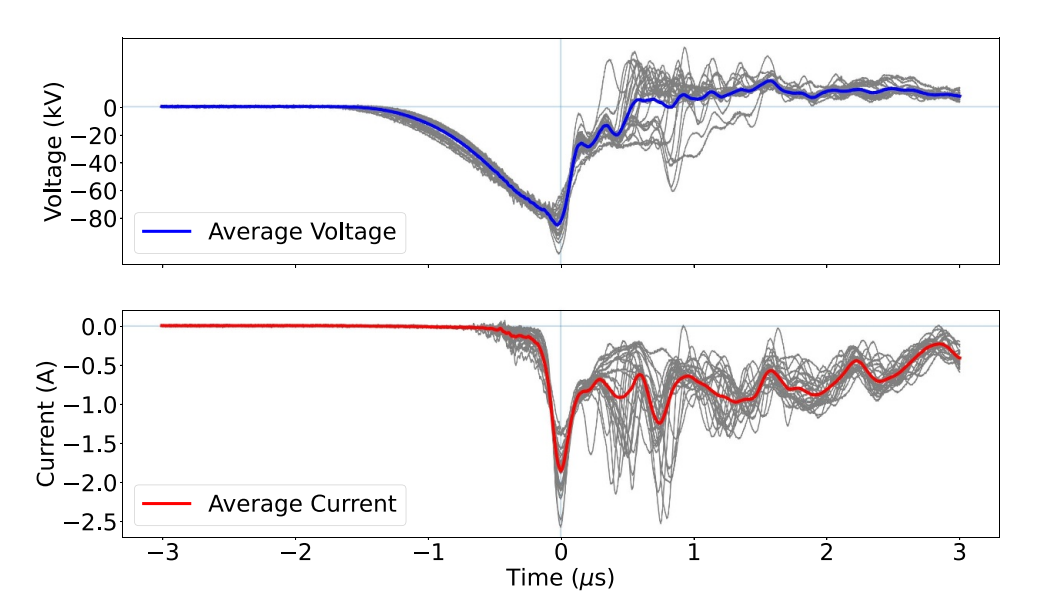


Figure 8. 25 spark discharges and their average voltage (blue) and current (red) from a past study of spark formation [6] and air resistance. The peak voltage in the spark study is 1.5 times greater than in this manuscript's streamer study. Notice that the peak current is about 20 times greater than in the streamer study which is consistent with spark formation. Moreover, the spark causes a voltage collapse not seen in figures 4, 5, or any of the supplementary figures provided in the repository. It is important to remember also that the breakdown voltage for a spark is 25 kV cm⁻¹ [11] which is 2.7 times larger than the average electric field across the gap for this streamer study (9 kV cm⁻¹).

ORCID ID

Luis Contreras-Vidal https://orcid.org/0000-0001-5461-7047

References

- [1] Bratchikov V, Gagarinov K, Kostyrya I, Tarasenko V, Tkachev A and Yakovlenko S 2007 X-ray radiation from the volume discharge in atmospheric-pressure air *Tech*. *Phys.* 52 856–64
- [2] Briels T, Kos J, Winands G, Veldhuizen E and Ebert U 2008 Positive and negative streamers in ambient air: measuring diameter, velocity and dissipated energy J. Phys. D: Appl. Phys. 41 234004
- [3] Briels T M P, Veldhuizen E and Ebert U 2008 Time resolved measurements of streamer inception in air *IEEE Trans*. *Plasma Sci.* 36 908–9
- [4] Carlson B E, Østgaard N, Kochkin P, Grondahl Ø, Nisi R, Weber K, Scherrer Z and LeCaptain K 2015 Meter-scale spark x-ray spectrum statistics J. Geophys. Res. 120 11,191–202
- [5] Celestin S and Pasko V P 2011 Energy and fluxes of thermal runaway electrons produced by exponential growth of streamers during the stepping of lightning leaders and in transient luminous events *J. Geophys. Res.* 116 A03315
- [6] Contreras-Vidal L 2020 Initial results from precision spark resistance measurements (available at: https://agu.confex. com/agu/fm20/meetingapp.cgi/Paper/706969)

- [7] Contreras-Vidal L 2022 Production of runaway electrons and x-rays during streamer inception phase (https://doi.org/ 10.6084/m9.figshare.20523924.v4)
- [8] Contreras-Vidal L, Sonnenfeld R, da Silva C, Mcharg M, Jensen D, Harley J, Taylor L, Haaland R and Stenbaek-Nielsen H 2021 Relationship between sprite current and morphology J. Geophys. Res. 3 126
- [9] Diniz G, Rutjes C, Ebert U and Ferreira I S 2019 Cold electron runaway below the friction curve *J. Geophys. Res.* 124 189–98
- [10] Dwyer J R et al 2004 Measurements of x-ray emission from rocket-triggered lightning Geophys. Res. Lett. 31 5
- [11] Dwyer J R 2005 The initiation of lightning by runaway air breakdown *Geophys. Res. Lett.* **32** 20
- [12] Dwyer J, Saleh Z, Rassoul H, Concha D, Rahman M, Cooray V, Jerauld J, Uman M and Rakov V 2008 A study of x-ray emission from laboratory sparks in air at atmospheric pressure J. Geophys. Res. 12 113
- [13] Eack K, Beasley W, Rust W, Marshall T and Stolzenburg M 1996 Initial results from simultaneous observation of x rays and electric fields in a thunderstorm *J. Geophys. Res.* 101 29637–40
- [14] Ebert U, Montijn C, Briels T, Hundsdorfer W, Meulenbroek B, Rocco A and Veldhuizen E 2006 The multiscale nature of streamers *Plasma Sources Sci. Technol.* 15 S118
- [15] Gurevich A V 1960 On the theory of runaway electrons Zh. Eksp. Teor. Fiz. (available at: www.osti.gov/biblio/ 4096516)
- [16] Howard J, Uman M A, Dwyer J R, Hill D, Biagi C, Saleh Z, Jerauld J and Rassoul H K 2008 Co-location of lightning leader x-ray and electric field change sources *Geophys. Res.* Lett. 35 L13817

- [17] Kochkin P, APJ van D and Ebert U 2015 Experimental study on hard x-rays emitted from metre-scale negative discharges in air J. Phys. D: Appl. Phys. 48 025205
- [18] Kochkin P O, Nguyen C V, APJ van D and Ebert U 2012 Experimental study of hard x-rays emitted from metre-scale positive discharges in air J. Phys. D: Appl. Phys. 45 425202
- [19] Longcope D 2019 Capacitance of a sphere near a ground plane - images charges to infinity (available at: http://solar. physics.montana.edu/dana/ph519/sph_cap.pdf)
- [20] Moore C B, Eack K B, Aulich G D and Rison W 2001 Energetic radiation associated with lightning stepped-leaders *Geophys. Res. Lett.* 28 2141–4
- [21] Moss G D, Pasko V P, Liu N and Veronis G 2006 Monte Carlo model for analysis of thermal runaway electrons in streamer tips in transient luminous events and streamer zones of lightning leaders J. Geophys. Res. 111 A02307
- [22] Nijdam S, Miermans K, van Veldhuizen E M, Ebert U and Peculiar Streamer A 2011 Morphology created by a complex voltage pulse *IEEE Trans. Plasma Sci.* 39 2216–7
- [23] Nijdam S, Teunissen J and Ebert U 2020 The physics of streamer discharge phenomena *Plasma Sources Sci. Technol.* 29 103001
- [24] Pantuso J G, da Silva C L, Sanchez J T and Bowers G S 2022 Geant4 simulations of x-ray photon pileup produced by runaway electrons in streamer discharges *Phys. Plasmas* 29 053506
- [25] Pasko V P 2007 Red sprite discharges in the atmosphere at high altitude: the molecular physics and the similarity with laboratory discharges *Plasma Sources Sci. Technol.* 16 S13–S29
- [26] Rahman M, Cooray V, Ahmad N A, Nyberg J, Rakov V A and Sharma S 2008 X rays from 80-cm long sparks in air Geophys. Res. Lett. 35 L06805
- [27] Shao T, Zhang C, Niu Z, Yan P, Tarasenko V F, Baksht E K, Burahenko A G and Shut'ko Y V 2011 Diffuse discharge,

- runaway electron and x-ray in atmospheric pressure air in an inhomogeneous electrical field in repetitive pulsed modes *Appl. Phys. Lett.* **98** 021503
- [28] Shao T, Zhang C, Niu Z, Yan P, Tarasenko V F, Baksht E K, Kostyrya I D and Shutko V 2011 Runaway electron preionized diffuse discharges in atmospheric pressure air with a point-to-plane gap in repetitive pulsed mode *J. Appl. Phys.* 109 083306
- [29] da Silva C L, Sonnenfeld R G, Edens H E, Krehbiel P R, Quick M G and Koshak W J 2019 The plasma nature of lightning channels and the resulting nonlinear resistance J. Geophys. Res. 124 9442–63
- [30] da Silva C, Millan R, Mcgaw D, Yu C, Putter A, LaBelle J and Dwyer J 2017 Laboratory measurements of x-ray emissions from centimeter-long streamer corona discharges *Geophys*. *Res. Lett.* 10 44
- [31] da Silva C and Pasko V 2013 Dynamics of streamer-to-leader transition at reduced air densities and its implications for propagation of lightning leaders and gigantic jets *J. Geophys. Res.* 12 118
- [32] Starikovskiy A Y, Aleksandrov N L and Shneider M N 2021 Simulation of decelerating streamers in inhomogeneous atmosphere with implications for runaway electron generation J. Appl. Phys. 129 063301
- [33] Tarasenko V 2020 Runaway electrons in diffuse gas discharges *Plasma Sources Sci. Technol.* 29 034001
- [34] Tardiveau P, Moreau N, Bentaleb S, Postel C and Pasquiers S 2009 Diffuse mode and diffuse-to-filamentary transition in a high pressure nanosecond scale corona discharge under high voltage J. Phys. D: Appl. Phys. 42 175202
- [35] Zhang C, Shao T, Yu Y, Niu Z, Yan P and Zhou Y 2010 Detection of x-ray emission in a nanosecond discharge in air at atmospheric pressure *Rev. Sci. Instrum.* **81** 123501